

Article

# Particle Size and PdO–Support Interactions in PdO/CeO<sub>2</sub>- $\gamma$ Al<sub>2</sub>O<sub>3</sub> Catalysts and Effect on Methane Combustion

Domenica R. Fertal <sup>1</sup>, Maxim P. Bukhovko <sup>2</sup>, Yong Ding <sup>3</sup>, Mehmet Z. Billor <sup>4</sup> and Anil C. Banerjee <sup>1,\*</sup> 

<sup>1</sup> Department of Chemistry, Columbus State University, Columbus, GA 31907, USA; fertal\_domenica@columbusstate.edu

<sup>2</sup> Department of Chemical and Biomolecular Engineering, Georgia Institute of Technology, Atlanta, GA 30332, USA; maxim.bukhovko@gatech.edu

<sup>3</sup> School of Materials Science and Engineering, Georgia Institute of Technology, Atlanta, GA 30332, USA; yong.ding@gatech.edu

<sup>4</sup> Department of Geosciences, Auburn University, Auburn, AL 36849, USA; mzb0009@auburn.edu

\* Correspondence: banerjee\_anil@columbusstate.edu; Tel.: +1-706-569-3030

Received: 25 July 2020; Accepted: 26 August 2020; Published: 30 August 2020



**Abstract:** In this study, we investigated the effects of sequential impregnation in two PdO/CeO<sub>2</sub>/Al<sub>2</sub>O<sub>3</sub> nanocatalysts (4Pd-20CeO<sub>2</sub>/Al<sub>2</sub>O<sub>3</sub> and 20CeO<sub>2</sub>-4Pd/Al<sub>2</sub>O<sub>3</sub>) on catalytic properties, particle sizes, and metal oxide–support interactions. Pulse chemisorption indicated significantly higher dispersion and smaller particle size in the 20CeO<sub>2</sub>-4Pd/Al<sub>2</sub>O<sub>3</sub> catalyst. STEM images of the 4Pd-20CeO<sub>2</sub>/Al<sub>2</sub>O<sub>3</sub> catalyst showed PdO nanoparticles on the surface of crystalline Al<sub>2</sub>O<sub>3</sub>. In the 20CeO<sub>2</sub>-4Pd/Al<sub>2</sub>O<sub>3</sub> catalyst, PdO nanoparticles were strongly embedded on ceria indicating PdO-ceria interactions. Both supports were on separate sites in the two catalysts suggesting weak interactions. PdO particle sizes were 6–12 nm in the 4Pd-20CeO<sub>2</sub>/Al<sub>2</sub>O<sub>3</sub> catalyst and 4–8 nm in the 20CeO<sub>2</sub>-4Pd/Al<sub>2</sub>O<sub>3</sub> catalyst. Methane conversion was 100% at 275 °C after a 20-min run with the 4Pd-20CeO<sub>2</sub>/Al<sub>2</sub>O<sub>3</sub> catalyst compared to 25% conversion by the 20CeO<sub>2</sub>-4Pd/Al<sub>2</sub>O<sub>3</sub> catalyst under same conditions. The support alumina could stabilize the PdO species and facilitated oxygen migration on the surface and from the bulk in the 4Pd-20CeO<sub>2</sub>/Al<sub>2</sub>O<sub>3</sub> catalyst. The lower activities in the 20CeO<sub>2</sub>-4Pd/Al<sub>2</sub>O<sub>3</sub> catalyst could be due to inaccessibility of PdO active sites at low temperature due to embedment of PdO nanoparticles on ceria. We could infer from our data that sequence of impregnation in catalyst synthesis could significantly influence catalytic properties and methane combustion due to PdO–support interactions.

**Keywords:** sequential impregnation; catalyst preparation method; PdO–support interactions; particle size; particle size distribution; methane combustion

## 1. Introduction

Catalytic combustion of methane has generated immense interests for development of industrial processes for pollution control as well as for understanding the mechanism of the catalytic reactions. Two recent reviews [1,2] summarized the recent advances made in the catalytic combustion of methane. Methane combustion by palladium catalysts on different supports including alumina [3–5], ceria [6,7] and ceria-alumina have been reported [8–12]. Preparation of palladium catalysts on ceria-alumina supports by different methods have reported including impregnation [9–15], sol-gel [10], supramolecular approach [8], and atomic layer deposition [16]. Li et al. [9] made Pd/CeO<sub>2</sub>/Al<sub>2</sub>O<sub>3</sub> nanocatalysts by adding aqueous cerium nitrate hexahydrate to a suspension of Pd nanoparticles in water, followed by mixing with Al<sub>2</sub>O<sub>3</sub>. Liu et al. [13] prepared Pd/CeO<sub>2</sub>/Al<sub>2</sub>O<sub>3</sub> catalysts by

impregnating aqueous cerium nitrate hexahydrate solution to  $\gamma$ - $\text{Al}_2\text{O}_3$  followed by addition to an aqueous solution of  $\text{PdCl}_2$  under ultrasonic irradiation. Yang et al. [14] prepared a  $\text{PdO}/\text{CeO}_2/\text{Al}_2\text{O}_3$  by adding an aqueous suspension of  $\text{Pd}/\text{CeO}_2$  colloidal spheres to  $\text{Al}_2\text{O}_3$ . Sun et al. [12] prepared  $\text{PdO}/\text{CeO}_2/\text{Al}_2\text{O}_3$  catalysts by changing the loading sequence of  $\text{CeO}_2$  and Pd over  $\text{Al}_2\text{O}_3$ .

Several researchers reported activity results with Pd catalysts on alumina-ceria supports. Cargnello et al. [8] reported exceptional activity by a catalyst made of modular  $\text{Pd}/\text{CeO}_2$  subunits functionalized on  $\text{Al}_2\text{O}_3$  for methane combustion. Li et al. [9] reported 90% hydrocarbon conversion at 320 °C with  $\text{Pd}/\text{CeO}_2/\text{Al}_2\text{O}_3$  nanocatalysts. Ramirez-Lopez et al. [10] investigated the complete catalytic oxidation of methane by varying ceria loading in  $\text{Pd}/\text{CeO}_2$ - $\text{Al}_2\text{O}_3$  catalysts and found high ceria loading decreased the catalytic activity. Rodrigues et al. [11] found that addition of ceria improved activity and stability of a  $\text{Pd}/\text{CeO}_2/\text{Al}_2\text{O}_3$  catalyst for partial methane oxidation. Sun et al. [12] investigated the effect of loading sequence in  $\text{Pd}/\text{CeO}_2/\text{Al}_2\text{O}_3$  catalysts on conversion of unburned hydrocarbons, carbon monoxide, and nitrogen oxides.

Another area that has received considerable attention is the effect of particle size, catalyst-support interfaces, and catalyst-support interactions in general, and for methane oxidation in particular. In a recent review, Monai et al. [2] included some studies showing Pd-support interactions at high dispersion and low Pd loading, while at higher Pd loadings, the methane conversion was higher and structure insensitive. In another review, Liu and Corma [17] summarized that particle size, shape, chemical composition and metal-support interaction could significantly influence the properties of metal catalysts. The interaction between nanoparticles and supports interaction and its effect on catalytic activity depends on the type, structure, and composition of the support [18].

A review of literature on catalytic combustion of methane using  $\text{Pd}/\text{CeO}_2/\text{Al}_2\text{O}_3$  catalysts provides conflicting results. Several studies also indicated that preparation methods could have significant effects on catalytic properties and activities. However, the area that has not been studied well is the synthesis of catalysts by changing the order of impregnation and the impact of such preparation on catalytic properties and activities. As a concept, such an innovative method could have great promise since it could alter the surface morphology and availability of active sites for catalytic reactions. In particular, it will be interesting to synthesize  $\text{Pd}/\text{CeO}_2/\text{Al}_2\text{O}_3$  catalysts by changing the order of loading of Pd, ceria, and alumina and study the effects of such preparation methods on catalytic properties and methane combustion at low temperatures. We did some preliminary experiments on synthesizing  $\text{Pd}/\text{CeO}_2/\text{Al}_2\text{O}_3$  catalysts by impregnating palladium nitrate on  $\text{CeO}_2/\text{Al}_2\text{O}_3$  and cerium nitrate on  $\text{Pd}/\text{Al}_2\text{O}_3$ , followed by activity experiments on methane combustion. Results showed substantial changes in properties and activities of the catalysts. Hence, we decided to conduct detailed investigations on this project. Our initial hypothesis was that the innovative synthesis method could alter the surface morphology and catalytic activities due to changes in Pd/PdO-support interactions. If the hypothesis is correct, the synthesis method would have a substantial impact in at least two ways. First, this will open up a new possibility of altering catalytic properties; secondly, such catalysts with different surface properties could have some future potentials on catalytic combustion of hydrocarbons and carbon monoxide at lower temperatures and thereby reducing and abetting air pollution caused by these pollutants. The project could also help us understand the mechanism by which the orders of impregnation in catalyst preparation alter catalytic properties and activities.

## 2. Results

### 2.1. Catalysis Synthesis

The details of the synthesis method and catalyst composition are described in the Materials and Methods section and also in Supplementary Materials. The two catalysts were designated as  $4\text{Pd}-20\text{CeO}_2/\text{Al}_2\text{O}_3$  and  $20\text{CeO}_2-4\text{Pd}/\text{Al}_2\text{O}_3$  to indicate the sequence of impregnation. The loading of Pd and ceria were arbitrarily chosen to be 4% and 20%, respectively, to make the components of

the catalysts more easily detectable. Both of these components are costly, and we will be looking into synthesizing these catalysts with a lower loading in the future.

### 2.2. Inductively Coupled Plasma Optical Emission Spectrometry (ICP-OES)

The palladium content was analyzed by ICP-OES method. The catalysts, 4Pd-20CeO<sub>2</sub>/Al<sub>2</sub>O<sub>3</sub> and 20CeO<sub>2</sub>-4Pd/Al<sub>2</sub>O<sub>3</sub>, contained 3.93 and 3.54 wt.% Pd respectively (Table 1). We thought it would be reasonable to round the Pd concentration to 4 wt.% Pd. For simplicity, 4 wt.% Pd was abbreviated as 4Pd in designating the two catalysts.

**Table 1.** Properties of the catalysts.

Properties	Catalysts	
	4Pd-20CeO <sub>2</sub> /Al <sub>2</sub> O <sub>3</sub>	20CeO <sub>2</sub> -4Pd/Al <sub>2</sub> O <sub>3</sub>
Pd wt.% (ICP-OES)	3.93	3.54
Surface Area (m <sup>2</sup> /g)	117	116
CO uptake in chemisorption	38.3 μmol/g	87.4 μmol/g
Dispersion	10.2%	26.4%
Metal Surface Area	1.8 m <sup>2</sup> /g	4.1 m <sup>2</sup> /g
Nanoparticle diameter (hemisphere)	10.9 nm	4.2 nm

### 2.3. X-Ray Photoelectron Spectroscopy (XPS)

The ex-situ XPS experiments were performed with the fresh catalysts and also with the spent catalysts after the combustion reaction with methane for 3 h. The ex-situ XPS results for the two catalysts in the Pd3d and Ce3d regions are shown in Figure 1 and Figure S3. The XPS data (Figure S4) shows the binding energies for the two catalysts before and after reaction.

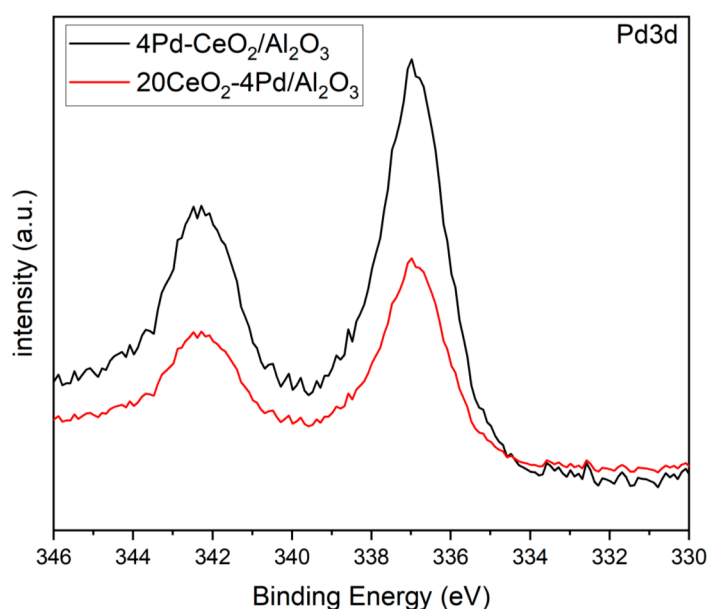


**Figure 1.** XPS in Pd3d regions of the two catalysts.

### 2.4. X-Ray Diffraction (XRD)

The XRD data for the two catalysts, PdO and the supports are given in Figure 2. The sharp 2-theta value at 32° was a characteristic XRD peak for PdO; the other peaks at 28°, 47° and 56° were for CeO<sub>2</sub> and the peak at 68° belonged to γ-Al<sub>2</sub>O<sub>3</sub>. Our results were in agreement with reported values [10,11,15].

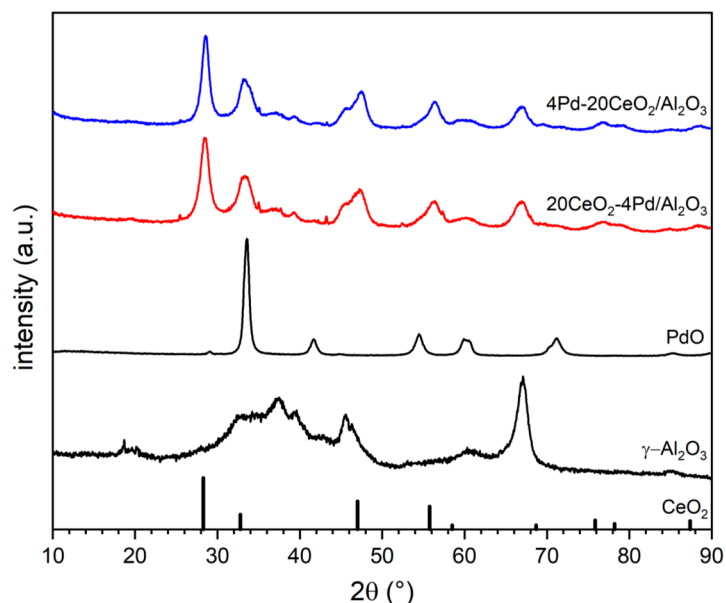


**Figure 2.** XRD of two catalysts, PdO and the supports.

### 2.5. Properties of the Catalysts

The properties of the two catalysts are given in Table 1. The surface area in the two catalysts were similar indicating that the sequence of impregnation did not affect the surface areas of the catalysts. Two noticeable differences in dispersion and particle size were found between 4Pd-20CeO<sub>2</sub>/Al<sub>2</sub>O<sub>3</sub> and 20CeO<sub>2</sub>-4Pd/Al<sub>2</sub>O<sub>3</sub> catalysts. The catalyst 20CeO<sub>2</sub>-4Pd/Al<sub>2</sub>O<sub>3</sub> prepared by impregnating ceria on Pd/Al<sub>2</sub>O<sub>3</sub> had 26% dispersion and average particle diameter of 4 nm compared to 10% dispersion and 11 nm particle diameter in the 4Pd-20CeO<sub>2</sub>/Al<sub>2</sub>O<sub>3</sub> catalyst prepared by impregnating PdO on the dual support of CeO<sub>2</sub>-Al<sub>2</sub>O<sub>3</sub>. Our data was in agreement with those reported by Sun et al. [12].

### 2.6. Hydrogen–Temperature Programmed Reduction (H<sub>2</sub>-TPR)

Figure 3 shows the H<sub>2</sub>-TPR profiles of the two catalysts. The measurements gave a negative peak at 50 °C, two strong peaks at 200 °C and 225 °C, and a small peak at around 780 °C.

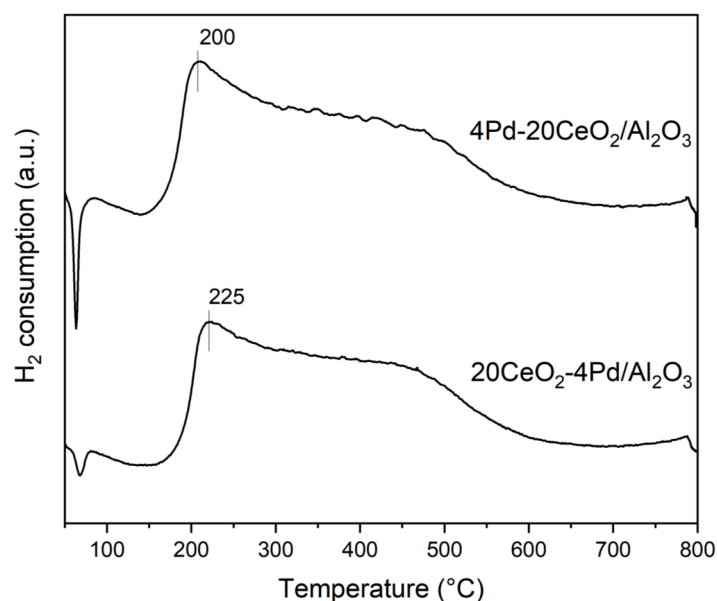


**Figure 3.** Hydrogen-TPR of the two catalysts.

## 2.7. High-Angle Annular Dark-Field Scanning Transmission Electron Microscopy (HAADF-STEM), Scanning Electron Microscopy (SEM), and Energy Dispersive Spectroscopy (EDS)

### 2.7.1. Location of PdO Particles on The Supports

HAADF-STEM, SEM, and EDS measurements were performed with the fresh catalysts and also with the spent catalysts after the combustion reaction with methane for 3 h. We used HAADF-STEM/SEM/EDS to identify the location of PdO particles on ceria/alumina supports. The HAADF-STEM images and EDS mapping are displayed in Figure 4 and Figure S5 for the 4Pd-20CeO<sub>2</sub>/Al<sub>2</sub>O<sub>3</sub> catalyst before methane combustion. These STEM images and EDS mapping indicated the following features: (i) most of the PdO nanoparticles were on the surface of the alumina support; (ii) there were virtually no PdO particles on the ceria support; (iii) most of the ceria and alumina particles were on separate sites; (iv) there were a few ceria particles overlapped with the alumina particles; (v) there were no PdO particles on ceria-alumina overlapped areas.

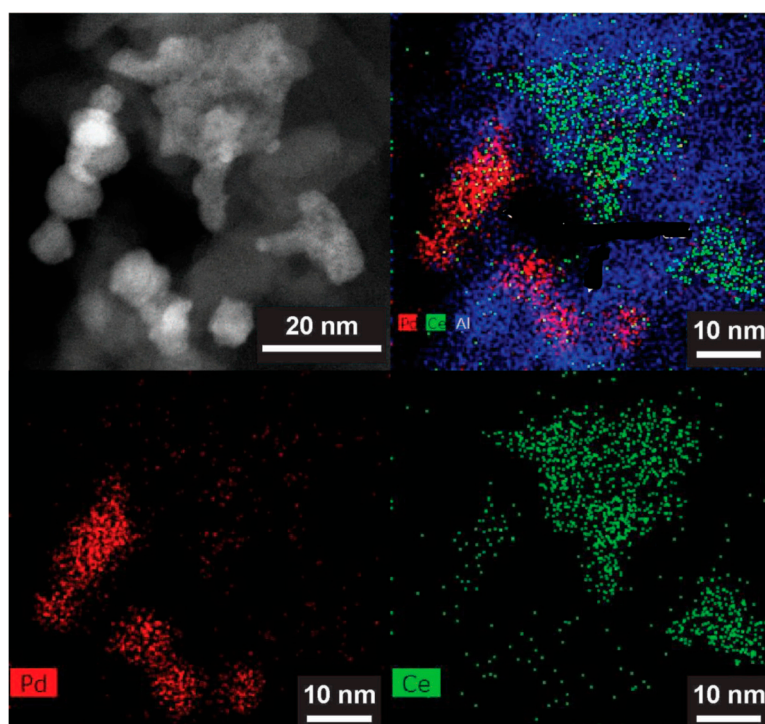


**Figure 4.** HAADF-STEM image and EDS mapping of 4Pd-20CeO<sub>2</sub>/Al<sub>2</sub>O<sub>3</sub> catalyst. (top left) STEM image; (top right) EDS overlapped mapping; (bottom left) EDS mapping of Pd; (bottom right) EDS mapping of Ce. Pd, Ce, and Al are color coded as red, green, and blue, respectively.

HAADF-STEM images and EDS mapping for the 4Pd-20CeO<sub>2</sub>/Al<sub>2</sub>O<sub>3</sub> catalyst after methane combustion are shown in Figure 5 and Figure S6. These images and mapping indicated the following features in the catalyst post reaction: (i) most of the PdO nanoparticles remained on the surface of the alumina support; (ii) most of the ceria and alumina particles were on separate sites; (iii) there were some PdO particles on ceria shown in the area with overlap of Pd and Ce signals (Figure S6).

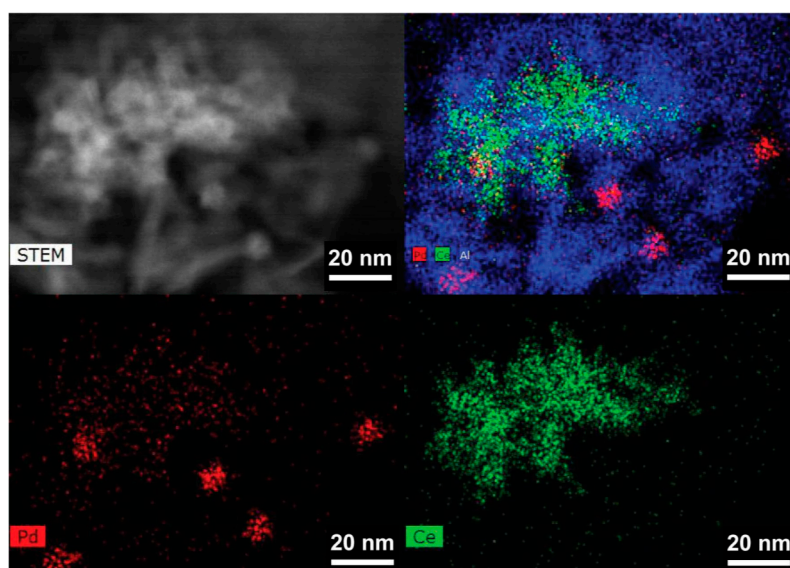


**Figure 5.** HAADF-STEM image and EDS mapping of 4Pd-20CeO<sub>2</sub>/Al<sub>2</sub>O<sub>3</sub> catalyst (post reaction). (**top left**) STEM image; (**top right**) elementary distribution of Pd, Ce, Al overlapped together; (**bottom left**) EDS mapping to show elementary distribution of Pd; (**bottom right**) EDS mapping to show elementary distribution of Ce. Pd, Ce, and Al are color coded as red, green, and blue, respectively.

Figures 6 and 7 display the HAADF-STEM images and EDS mapping for the 20CeO<sub>2</sub>-4Pd/Al<sub>2</sub>O<sub>3</sub> catalyst before and after reaction, respectively. There was a major change in the location of PdO particles in 4Pd-20CeO<sub>2</sub>/Al<sub>2</sub>O<sub>3</sub> and 20CeO<sub>2</sub>-4Pd/Al<sub>2</sub>O<sub>3</sub> catalysts before reaction (Figures 4 and 6). Most of the PdO nanoparticles in the 20CeO<sub>2</sub>-4Pd/Al<sub>2</sub>O<sub>3</sub> catalyst were embedded on the surface of the ceria in contrast to most PdO particles being on the surface of alumina in 4Pd-20CeO<sub>2</sub>/Al<sub>2</sub>O<sub>3</sub> catalyst.

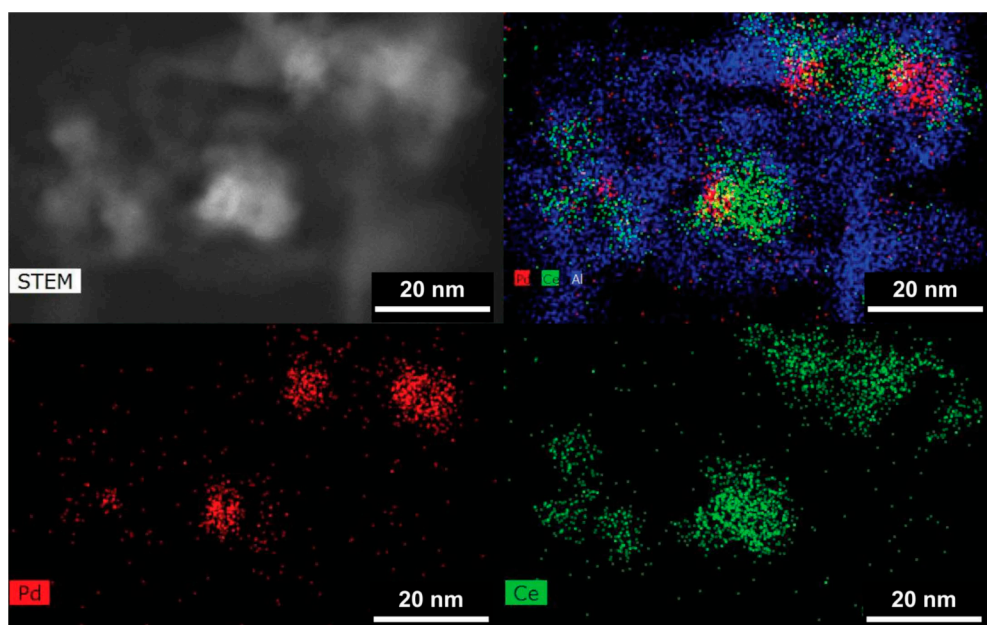


**Figure 6.** HAADF-STEM image and EDS mapping of 20CeO<sub>2</sub>-4Pd/Al<sub>2</sub>O<sub>3</sub> catalyst. (**top left**) STEM image; (**top right**) elementary distribution of Pd, Ce, Al overlapped together; (**bottom left**) EDS mapping to show elementary distribution of Pd; (**bottom right**) EDS mapping to show elementary distribution of Ce. Pd, Ce, and Al are color coded as red, green, and blue, respectively.

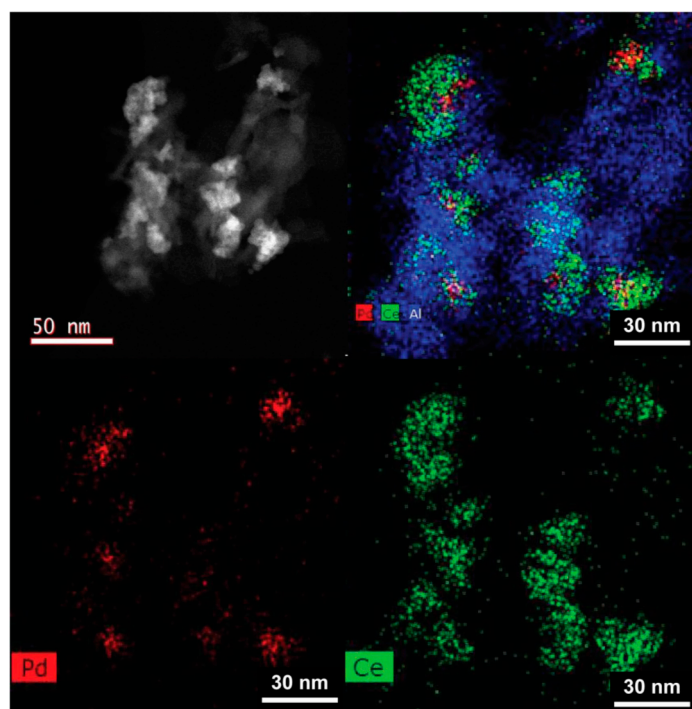


**Figure 7.** HAADF-STEM image and EDS mapping of 20CeO<sub>2</sub>-4Pd/Al<sub>2</sub>O<sub>3</sub> catalyst (post reaction). **(top left)** STEM image; **(top right)** elementary distribution of Pd, Ce, Al overlapped together; **(bottom left)** EDS mapping to show elementary distribution of Pd; **(bottom right)** EDS mapping to show elementary distribution of Ce. Pd, Ce, and Al are color coded as red, green, and blue, respectively.

There were not many differences in the location of PdO particles in the 20CeO<sub>2</sub>-4Pd/Al<sub>2</sub>O<sub>3</sub> catalyst before and after reaction except that some PdO particles were on the ceria-alumina interface after the reaction (Figure 7).

### 2.7.2. Morphology and PdO–Support Interactions

The morphology and PdO–support interactions of the catalysts before and after reaction were assessed from the STEM and SEM images shown in Figure 8 and Figures S7–S10.

### 2.7.3. Particle Sizes and Distribution

The particle sizes were calculated with Gatan Micrograph Software (GMS). The PdO particle sizes are shown in Figures S11–S14. The particle size range was 6–12 nm in the 4Pd-20CeO<sub>2</sub>/Al<sub>2</sub>O<sub>3</sub> catalyst before and after reaction (Figures S11 and S12). The particle size range in the 20CeO<sub>2</sub>-4Pd/Al<sub>2</sub>O<sub>3</sub> catalyst was 4–8 nm before reaction (Figure S13) and 4–10 nm after reaction. The particle size distributions are shown in Figure 9.

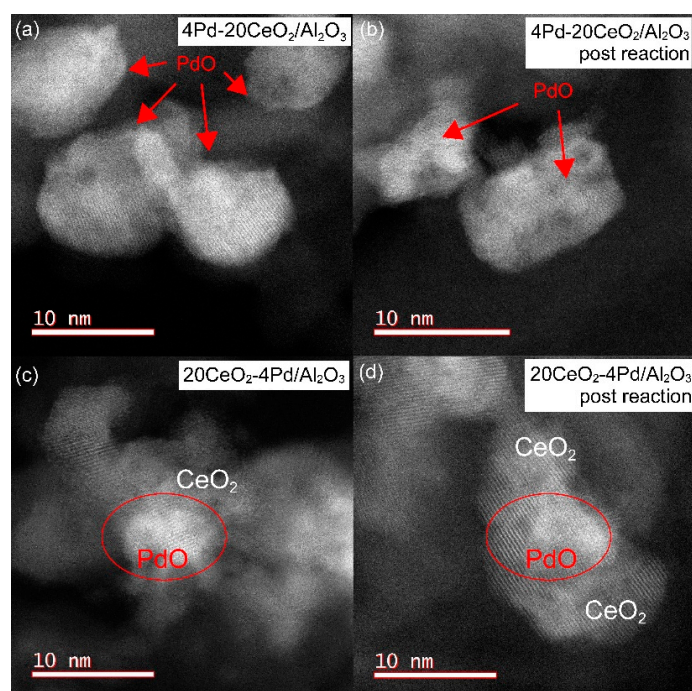


**Figure 8.** Morphology of 4Pd-20CeO<sub>2</sub>/Al<sub>2</sub>O<sub>3</sub> and 20CeO<sub>2</sub>-4Pd/Al<sub>2</sub>O<sub>3</sub> catalysts before and after reaction. (a) PdO particles are on alumina (black background) before reaction; (b) Pd particles are on alumina (black background) after reaction; (c) PdO particles are embedded on ceria before reaction; (d) Pd particles are embedded on ceria after reaction.

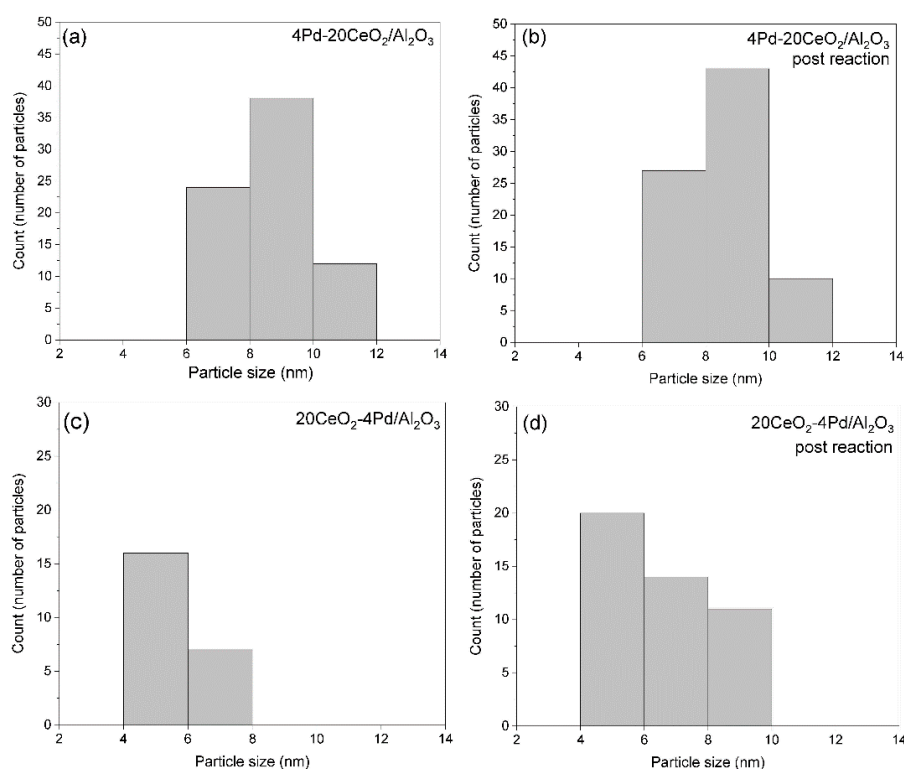


**Figure 9.** Particle size distributions. (a) PdO particle size distribution in 4Pd-20CeO<sub>2</sub>/Al<sub>2</sub>O<sub>3</sub> before reaction; (b) PdO particle size distribution in 4Pd-20CeO<sub>2</sub>/Al<sub>2</sub>O<sub>3</sub> after reaction; (c) PdO particle size distribution in 20CeO<sub>2</sub>-4Pd/Al<sub>2</sub>O<sub>3</sub> before reaction; (d) PdO particle size distribution in 20CeO<sub>2</sub>-4Pd/Al<sub>2</sub>O<sub>3</sub> after reaction.

## 2.8. Activity of the Catalysts

The activities of the two catalysts are given in Figure 10. Activity experiments were carried out in the temperature range of 200–450 °C. Each experiment was performed for 20 min with a gas hourly space velocity of 45,000 (cc/g. catalyst), h<sup>-1</sup>. Each activity experiment was repeated at least three times at each temperature and conversion data within 2–3% deviations were only accepted. Each datapoint in Figure 10 represents the average value of three runs at a temperature. The oxidation of methane was initiated within the temperature range of 200–210 °C and reached 40% conversion at 225 °C and then 100% conversion at 275 °C in the 4Pd-20CeO<sub>2</sub>/Al<sub>2</sub>O<sub>3</sub> catalyst. The conversion remained at 100% in the temperature range 275–450 °C indicating thermal stability of the catalyst in this temperature range. For the 20CeO<sub>2</sub>-4Pd/Al<sub>2</sub>O<sub>3</sub> catalyst, the catalytic reaction was initiated at around 250 °C and reached 25% conversion at 275 °C and then reaching 100% conversion at 350 °C. The conversion remained at 100% in the temperature range 350–450 °C indicating thermal stability of the catalyst in this temperature range. While long term stability tests were not performed, each catalyst was able to withstand multiple runs for a duration of 6 h and did not show any decrease in activity or noticeable change in the morphology. The effluent gas mixture contained water, carbon dioxide, unconverted methane, oxygen, and nitrogen. Water as a product was absorbed in a moisture trap and was not estimated. Unconverted methane and carbon dioxide were analyzed in a gas chromatograph. There was correlation between % methane reacted and % carbon dioxide produced as per the stoichiometric reaction for methane complete combustion. We did not find any peak for carbon monoxide in the gas chromatograph and this could be explained by the presence of excess oxygen in the oxygen-rich gas mix.

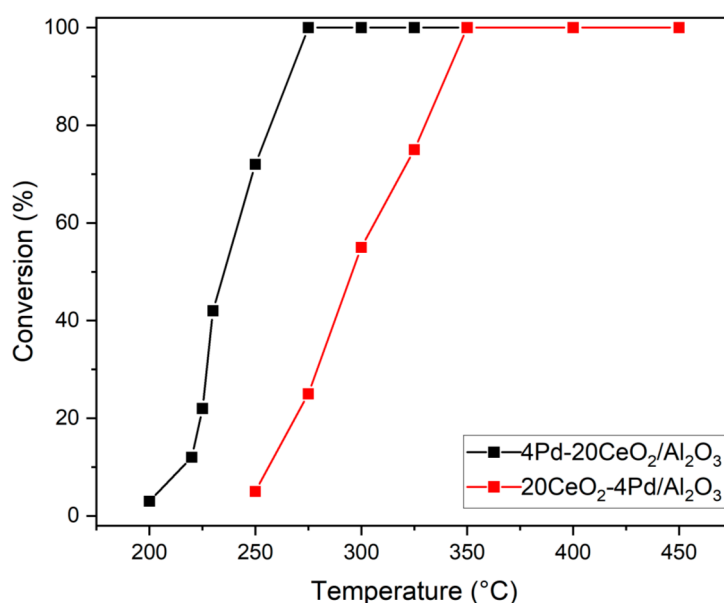


**Figure 10.** Methane conversion at different temperatures. [GHSV, 45,000 (cc/g.cat) h<sup>-1</sup>; reaction time at each temperature, 20 min; inlet gas mix composition, 1.0% CH<sub>4</sub>, 4.0% O<sub>2</sub>, balance N<sub>2</sub>].

## 2.9. Activation Energy

Figure 11 gives the Arrhenius plot on the activation energies for the catalytic reaction with the two catalysts. Activation energies were determined in the kinetic regions of temperatures corresponding to methane conversions below 27%. Runs were repeated at least three times at each temperature and conversion data within 2–3% deviations only were accepted. Each datapoint in Figure 11 represents the average value of three runs at a temperature. The activation energies were 119 kJ/mol and 136 kJ/mol for the 4Pd-20CeO<sub>2</sub>/Al<sub>2</sub>O<sub>3</sub> and 20CeO<sub>2</sub>-4Pd/Al<sub>2</sub>O<sub>3</sub> catalysts, respectively.

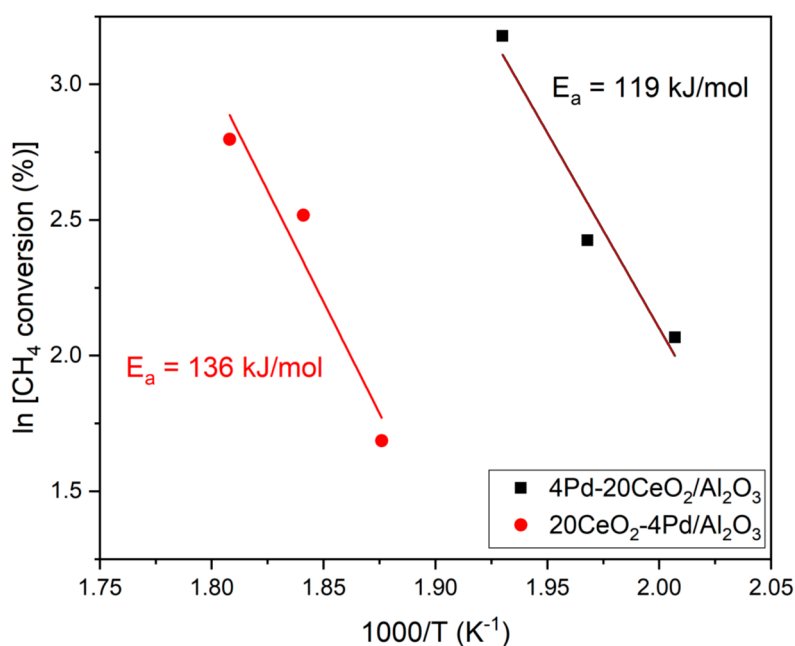


**Figure 11.** Activation energy for methane combustion with the two catalysts.

### 3. Discussion

The binding energies 337 eV and 342.5 eV in Figure 1 were assigned to PdO in both catalysts [7,15]. The lower intensity magnitude of the Pd3d signal for the 20CeO<sub>2</sub>-4PdAl<sub>2</sub>O<sub>3</sub> catalyst suggested that there were fewer Pd species exposed on the surface. This observation was also consistent with our STEM analysis of the catalyst, which found several examples of PdO nanoparticles embedded within the ceria. The centers and positions of the Pd3d peaks for both catalysts were nearly identical, suggesting that the surface PdO species had similar oxidation states in both catalysts. The binding energies 917.5 eV, 897.0 eV, and 882.5 eV in Figures S3 and S4b,d in the Ce3d regions were for Ce<sup>4+</sup> in CeO<sub>2</sub>. There were no clear changes in the XPS spectra in Figure S4a, suggesting that the oxidation states of Pd and Pd concentration did not change after reaction with methane in the 4Pd-20CeO<sub>2</sub>/Al<sub>2</sub>O<sub>3</sub> catalyst. XPS analysis of 20CeO<sub>2</sub>-4PdAl<sub>2</sub>O<sub>3</sub> catalyst after reaction (Figure S4c) also suggests that there were less PdO species on the surface as the signal intensity for the Pd3d spectrum was much lower compared to that of the fresh catalyst. The STEM analysis also supported this observation with the changes in PdO-ceria interface within the particles and some embedded PdO.

The XPS results confirmed the presence of PdO on the surface of the supports and that ceria was present as CeO<sub>2</sub>. Our results were in agreement with data previously reported [5–7,19]. Based on the XPS and XRD data, we could confirm that the composition of the two catalysts was PdO, CeO<sub>2</sub>, and  $\gamma$ -Al<sub>2</sub>O<sub>3</sub>. We reported in a previous study with a Pd/ $\gamma$ -Al<sub>2</sub>O<sub>3</sub> catalyst that both PdO and PdOx were the active phases [5]. However, in this study with a PdO catalyst on dual support of ceria and alumina, we did not detect any Pd metal or PdOx as components in the two catalysts. The reason for the presence of PdO as the active phase in the catalysts is the synthesis method and calcination at a lower temperature of 500 °C. The purpose of this study was to develop a catalyst for low temperature combustion of methane. Hence, we conducted activity runs in the temperature range of 200–450 °C. Under these conditions, PdO is the stable phase and PdO decomposes to metallic Pd only above 800 °C. Collusi et al. [15] reported Pd-PdO transition with PdOx as the intermediate in the catalytic oxidation of methane with Pd/CeO<sub>2</sub>/Al<sub>2</sub>O<sub>3</sub> catalysts. Rodrigues et al. [10] also confirmed through XPS the active phase to be PdO in their studies with a Pd/CeO<sub>2</sub>/Al<sub>2</sub>O<sub>3</sub> catalyst for partial methane oxidation.

As reported in the results in Table 1, the two catalysts showed a large difference in both dispersion and particle sizes. Sun et al. [12] also observed similar trends with the two catalysts and argued that lower dispersion in the PdO/CeO<sub>2</sub>/Al<sub>2</sub>O<sub>3</sub> catalyst was due to PdO particles being fixed on ceria caused

by strong Pd-O-Ce bonds. Even though our dispersion results were similar to those reported by this research group, we did not see PdO deposition on ceria in the PdO/CeO<sub>2</sub>/Al<sub>2</sub>O<sub>3</sub> catalyst. Onn et al. [16] found the dispersion to be much higher in a PdO/CeO<sub>2</sub>/Al<sub>2</sub>O<sub>3</sub> catalyst prepared by atomic layer deposition method.

In the H<sub>2</sub>-TPR experiment, the negative peak at around 50 °C could be attributed to the decomposition of palladium hydride [5]. The peaks at 200 °C and 225 °C were attributed to the reduction of relatively large PdO particles under weak interaction with the support. The peak temperature was 25 °C lower in the 4Pd-20CeO<sub>2</sub>/Al<sub>2</sub>O<sub>3</sub> catalyst compared to the 20CeO<sub>2</sub>-4Pd/Al<sub>2</sub>O<sub>3</sub> catalyst, indicating weaker PdO-support interaction in the 4Pd-20CeO<sub>2</sub>/Al<sub>2</sub>O<sub>3</sub> catalyst. A small peak at around 780 °C could be due to reduction of bulk CeO<sub>2</sub> [14]. Sun et al. [12] observed peaks at 112 °C and 129 °C for the Pd/Ce/Al and Ce/Pd/Al catalysts and assigned these peaks to the reduction of PdO. Rodrigues et al. [10] reported two H<sub>2</sub>-TPR peaks at 110 °C and 330–345 °C in a 1% Pd–5% CeO<sub>2</sub>/Al<sub>2</sub>O<sub>3</sub> catalyst prepared by impregnation method. The first peak was attributed to the reduction of relatively large PdO particles under weak interaction with the support, whereas the second peak was due to the reduction of PdO particles under stronger interaction with the support. Ramirez-Lopez et al. [11] reported a H<sub>2</sub>-TPR peak at 380–420 °C for a 0.2% Pd/15% CeO<sub>2</sub>/Al<sub>2</sub>O<sub>3</sub> catalyst and attributed it to the reduction of surface oxygen of CeO<sub>2</sub>. Liu et al. [13] got two H<sub>2</sub>-TPR peaks with their Pd/CeO<sub>2</sub>-Al<sub>2</sub>O<sub>3</sub> catalyst and assigned the peak at 210 °C to desorption of H<sub>2</sub> adsorbed by Pd/PdO and the second peak at 580 °C to reduction of bulk CeO<sub>2</sub>.

The HAADF-STEM/SEM/EDS images (Figure 8 and Figures S7–S10) provided insights on the morphology and nature of PdO-support interactions in the two catalysts. PdO particles were crystalline and on the surface of  $\gamma$ -Al<sub>2</sub>O<sub>3</sub> in the 4Pd-20CeO<sub>2</sub>/Al<sub>2</sub>O<sub>3</sub> catalyst, whereas in the 20CeO<sub>2</sub>-4Pd/Al<sub>2</sub>O<sub>3</sub> catalyst, PdO particles (both crystalline and amorphous) were strongly embedded on ceria. The reason of PdO nanoparticles being embedded on ceria could be due to strong PdO-CeO<sub>2</sub> interactions through Pd-O-Ce bonds. After methane combustion, we detected some PdO-ceria overlap (Figure S6) indicating PdO-CeO<sub>2</sub> interactions in the 4Pd-20CeO<sub>2</sub>/Al<sub>2</sub>O<sub>3</sub> catalyst post-reaction. We also noticed that PdO particles were more amorphous and embedded on ceria in the 20CeO<sub>2</sub>-4Pd/Al<sub>2</sub>O<sub>3</sub> catalyst after the reaction (Figure S8), indicating changes in the morphology of the catalyst as a result of methane combustion reaction. Sun et al. [12] found that in the PdO/CeO<sub>2</sub>/Al<sub>2</sub>O<sub>3</sub> catalyst, PdO particles were in contact with CeO<sub>2</sub> and no dispersion of PdO nanoparticles on amorphous Al<sub>2</sub>O<sub>3</sub> was observed. In the second catalyst (CeO<sub>2</sub>/PdO/Al<sub>2</sub>O<sub>3</sub>), they detected PdO particles well-distributed and stabilized on both CeO<sub>2</sub> and Al<sub>2</sub>O<sub>3</sub> supports. These researchers interpreted their findings based on stronger Ce-O-Pd bonds compared to Al-O-Pd bonds. Our results and explanations are in contradiction to the findings of Sun et al. [12]. In our research, we also found that CeO<sub>2</sub> and Al<sub>2</sub>O<sub>3</sub> supports were mostly on separate sites and there was almost no overlap indicating weaker support-support interactions. The support could play an important role in controlling the size, shape, and structural stability of metal nanoparticles through metals-support interactions in chemical reactions. The support could also affect the reactivity of metal nanoparticles by changing chemical properties through strong metal-support interactions [18]. Huang et al. [20] studied the effect of calcination temperature on the performances of Pd/Al<sub>2</sub>O<sub>3</sub>-CeO<sub>2</sub> catalysts and observed that 1.9 nm Pd particles developed stronger Pd-Ce interaction and improved methane combustion. Lan et al. [21] studied the effect of synthesis method on the properties and catalytic performance of Pd/Ce<sub>0.5</sub>Zr<sub>0.5</sub>O<sub>2</sub>-Al<sub>2</sub>O<sub>3</sub> three-way catalysts. Murata et al. [22] investigated the relationship between the strength of the metal-oxygen bond of the support and the catalytic activity in methane combustion and found that PdO particles were strongly anchored by the supports (Al<sub>2</sub>O<sub>3</sub>, CeO<sub>2</sub>, and ZrO<sub>2</sub>) due to strong metal-oxygen bonding.

The particles sizes in the 4Pd-20CeO<sub>2</sub>/Al<sub>2</sub>O<sub>3</sub> catalyst were in the range of 6–12 nm before and after reaction from one area of EDS mapping (Figures S11 and S12). The particle sizes of PdO in the 20CeO<sub>2</sub>-4Pd/Al<sub>2</sub>O<sub>3</sub> catalyst before and after reaction from another area of EDS mapping are shown in Figures S13 and S14. The particle sizes ranged from 4–8 nm before reaction and 4–10 nm after reaction.

A comparison of the particle size distributions between the two catalysts (4Pd-20CeO<sub>2</sub>/Al<sub>2</sub>O<sub>3</sub> and 20CeO<sub>2</sub>-4Pd/Al<sub>2</sub>O<sub>3</sub>) provided some striking features (Figure 9). Most particles were in the size range of 6–12 nm in the 4Pd-20CeO<sub>2</sub>/Al<sub>2</sub>O<sub>3</sub> catalyst while the range was much smaller (4–8 nm) in the 20CeO<sub>2</sub>-4Pd/Al<sub>2</sub>O<sub>3</sub> catalyst. The PdO nanoparticles were strongly embedded in ceria resulting in portions of the spherical PdO particles not being exposed to the surface. This could explain the lower particle size range in the 20CeO<sub>2</sub>-4Pd/Al<sub>2</sub>O<sub>3</sub> catalyst. There were changes in the particle size distributions in the 20CeO<sub>2</sub>-4Pd/Al<sub>2</sub>O<sub>3</sub> catalyst after methane combustion with about 25% of PdO particles being in a higher range of 4–10 nm (Figure 9d). The increase in the particle size could be due to relatively weaker PdO-ceria interactions as a result of the combustion reaction and PdO particles being less embedded on ceria. The results indicated that the order of impregnation had a significant effect on particle sizes and distributions.

Murata et al. [23] investigated the effects of Pd particle sizes and Al<sub>2</sub>O<sub>3</sub> crystal phases on methane combustion under wet conditions using Pd/Al<sub>2</sub>O<sub>3</sub> catalysts. X-ray absorption fine structure (XAFS) data showed isolated Pd atoms and amorphous-like PdO particles in the Pd/Al<sub>2</sub>O<sub>3</sub> catalysts with smaller Pd particle sizes. STEM images showed amorphous-like PdO when particle sizes were less than 3 nm, and lattice fringes and crystalline PdO nanoparticles when sizes were more than 10 nm. Sun et al. [12] measured particle sizes by transmission electron microscopy (TEM) and reported particle size range (4–8 nm) for the Pd/Ce/Al catalyst compared to 2–6 nm particle sizes for the Ce/Pd/Al catalyst. Our results on particle size ranges are in some agreement with the results from this research group.

As reported in the results section, the 4Pd-20CeO<sub>2</sub>/Al<sub>2</sub>O<sub>3</sub> catalyst had better low temperature activities for methane combustion with 100% conversion at 275 °C in comparison to the same conversion at 350 °C by the 20CeO<sub>2</sub>-4Pd/Al<sub>2</sub>O<sub>3</sub> catalyst. Moreover, the activation energy of the methane combustion reaction was lower with the 4Pd-20CeO<sub>2</sub>/Al<sub>2</sub>O<sub>3</sub> catalyst compared to the reaction using the 20CeO<sub>2</sub>-4Pd/Al<sub>2</sub>O<sub>3</sub> catalyst. However, PdO dispersion was higher and PdO particle size was smaller in the 20CeO<sub>2</sub>-4Pd/Al<sub>2</sub>O<sub>3</sub> catalyst. Normally, as per Langmuir chemisorption, we should expect higher activities and lower activation energy for catalytic reactions with higher dispersion and lower particle size. This apparent anomaly in results could be explained by hypothesizing that the support alumina stabilized the PdO species and facilitated oxygen migration on the surface and from the bulk [24,25] in the 4Pd-20CeO<sub>2</sub>/Al<sub>2</sub>O<sub>3</sub> catalyst. Another plausible explanation for the lower activities with the 20CeO<sub>2</sub>-4Pd/Al<sub>2</sub>O<sub>3</sub> catalyst is as follows: the PdO sites were accessible for CO chemisorption, but not as active sites for the surface reaction with methane and oxygen since the PdO particles were embedded on ceria due to strong PdO-ceria interactions in the 20CeO<sub>2</sub>-4Pd/Al<sub>2</sub>O<sub>3</sub> catalyst. Sun et al. [12] reported 90% and 100% propane conversions at 323 °C and 340 °C, respectively, with a PdO/CeO<sub>2</sub>/Al<sub>2</sub>O<sub>3</sub> catalyst. Several researchers [9,13,14,26] reported 90% methane conversion at 320–500 °C with PdO/CeO<sub>2</sub>/Al<sub>2</sub>O<sub>3</sub> catalysts synthesized by different methods. Nilsson et al. [27] studied alumina and ceria supported palladium nanoparticles and found that reduced Pd sites or mixed Pd/PdO sites had high activity for methane oxidation. The catalytic activity could also change due to the redox behavior at the nanoscale due to presence of nonstoichiometric cerium oxides [28].

## 4. Materials and Methods

### 4.1. Catalyst Synthesis

The detailed methods of synthesis are given in the Supplementary Materials. A short description of the synthesis is given below.

- a. Synthesis of 4Pd-20CeO<sub>2</sub>/Al<sub>2</sub>O<sub>3</sub> catalyst: This catalyst was prepared by impregnating an aqueous solution of palladium nitrate hydrate to an aqueous slurry of the solid dual support of 20CeO<sub>2</sub>/Al<sub>2</sub>O<sub>3</sub> while vortexing for uniform mixing. The slurry was dried and calcined. The ICP-OES analysis gave Pd wt.% as 3.94. The final composition of the catalyst was rounded to 4.0 wt.% Pd (as PdO), 20 wt.% CeO<sub>2</sub> and 80 wt.%  $\gamma$ -Al<sub>2</sub>O<sub>3</sub> [designated in this article as 4Pd-20CeO<sub>2</sub>/Al<sub>2</sub>O<sub>3</sub>].

- b. Synthesis of 20CeO<sub>2</sub>-4Pd/Al<sub>2</sub>O<sub>3</sub> catalyst: This catalyst was prepared by impregnating an aqueous solution of cerium nitrate hexahydrate to an aqueous slurry of 5Pd/Al<sub>2</sub>O<sub>3</sub> while vortexing for uniform mixing. The slurry was dried and calcined. The ICP-OES analysis gave Pd wt.% as 3.56. The final composition of the catalyst was rounded to 20 wt.% CeO<sub>2</sub> and 4.0 wt.% Pd (as PdO) on  $\gamma$ -Al<sub>2</sub>O<sub>3</sub> [designated in this article as 20CeO<sub>2</sub>-4Pd/Al<sub>2</sub>O<sub>3</sub>].

#### 4.2. Activity Measurements

Activity measurements were conducted in a temperature-controlled horizontal fixed-bed flow reactor. The catalytic reactor unit (Figure S2) and the detailed procedure are described in the Supplementary Materials. The conversion of methane ( $v/v\%$ ) was calculated using the following equation:

$$\text{Conversion } (v/v\%) = \frac{[CH_4]_{in} - [CH_4]_{out}}{[CH_4]_{in}} \times 100\%$$

$CH_4$  <sub>in</sub> = Volume% of methane at 1 atm. and 25 °C in the gas feed entering the reactor.

$CH_4$  <sub>out</sub> = Volume% methane at 1 atm. and 25 °C in the gas mixture exiting the reactor.

#### 4.3. Activation Energy

Activation energies for the methane combustion with the two catalysts were determined in the kinetic regions of temperatures corresponding to methane conversions below 27%. The activation energy was calculated using the Arrhenius equation.

#### 4.4. Catalyst Characterization

- ICP-OES

Elemental analysis of Pd was conducted at Galbraith Laboratories, Inc. using inductively coupled plasma optical emission spectrometry (ICP-OES) by Perkin Elmer 5300V (Akron, OH, USA). The samples were prepared with a sodium peroxide fusion due to high% of Al<sub>2</sub>O<sub>3</sub>, followed by dissolution in water and acidification.

- XPS

Ex-situ X-ray photoelectron spectroscopy (XPS) analysis was performed with a Thermo K-Alpha spectrometer (ThermoFisher Scientific, Waltham, MA, USA), using a monochromatic Al K $\alpha$  radiation source. Spectra were measured in the regions of Pd3d, O1s, and Ce3d. Charge referencing was performed from the C1s region, referenced to the adventitious carbon (at 284.8 eV). The X-ray beam spot size was a 400  $\mu$ m and the spectrometer was operated at 50 eV pass energy and 50 ms dwell time for each step size of 0.1 eV.

- Chemisorption and Physisorption

Pulse CO chemisorption and temperature programmed reduction with hydrogen (TPR) and were performed in Micromeritics AutoChem II 2920 (Micromeritics Corporation, Norcross, GA, USA). Nitrogen physisorption was performed in a Micromeritics Tristar II (Micromeritics Corporation, Norcross, GA, USA). The detailed methods are described in the Supplementary Materials and also by Sulmonetti et al. [29].

- STEM, SEM and EDS

A Hitachi HD2700 (Hitachi Ltd., Tokyo, Japan) aberration-corrected scanning transmission electron microscope was used to record HAADF-STEM images, SEM images and EDS mappings. The samples were prepared on a lacey carbon-coated Au grid. More details on these techniques can be in a recent publication [30].

- XRD

For XRD data, a Bruker D2 Phaser Tabletop diffractometer (Bruker, Madison, WI, USA) was used with Cu-K $\alpha$  radiation at 30 kV and 10 mA, step size 0.02 (2 $\theta$ )/second and 10–90° (2 $\theta$ ).

## 5. Conclusions

We investigated the effects of sequence of impregnation in two PdO/CeO<sub>2</sub>/Al<sub>2</sub>O dual support nanocatalysts on particle sizes, metal oxide–support interactions, and catalytic activities for methane combustion. The composition of the two catalysts (4Pd-20CeO<sub>2</sub>/Al<sub>2</sub>O<sub>3</sub> and 20CeO<sub>2</sub>-4Pd/Al<sub>2</sub>O<sub>3</sub>) was 4 wt.% Pd as PdO, 20 wt.% CeO<sub>2</sub> and balance  $\gamma$ -Al<sub>2</sub>O<sub>3</sub>. The STEM images of the 4Pd-20CeO<sub>2</sub>/Al<sub>2</sub>O<sub>3</sub> catalyst showed that both supports were on separate sites and crystalline PdO nanoparticles were mostly on the surface of crystalline Al<sub>2</sub>O<sub>3</sub> before and after reaction. The PdO-alumina interaction was weak, and there was small PdO-CeO<sub>2</sub> interactions after reaction. In the 20CeO<sub>2</sub>-4Pd/Al<sub>2</sub>O<sub>3</sub> catalyst, PdO nanoparticles were embedded on ceria indicating strong PdO-ceria interactions. Moreover, the PdO nanoparticles became more amorphous and embedded on ceria and the PdO-ceria interface became more diffused after the reaction with this catalyst. Both supports were present on separate sites in the two catalysts suggesting weak support–support interactions between ceria and alumina. Another striking difference was in the particle size and particle size distribution in the two catalysts. Most particles were in the size range of 6–12 nm in the 4Pd-20CeO<sub>2</sub>/Al<sub>2</sub>O<sub>3</sub> catalyst while the range was lower (4–8 nm) in the 20CeO<sub>2</sub>-4Pd/Al<sub>2</sub>O<sub>3</sub> catalyst. The lower range could be due to strong PdO-ceria interactions making the particles partly hidden below the surface. There was an increase in the particle size range in the 20CeO<sub>2</sub>-4Pd/Al<sub>2</sub>O<sub>3</sub> catalyst after reaction, which may be due to relatively weaker PdO-ceria interactions as a result of the combustion reaction.

Activities of the two catalysts for methane combustion were also different. Methane conversion was 100% at 275 °C with the 4Pd-20CeO<sub>2</sub>/Al<sub>2</sub>O<sub>3</sub> catalyst compared to 25% conversion by the 20CeO<sub>2</sub>-4Pd/Al<sub>2</sub>O<sub>3</sub> catalyst at this temperature and under the same conditions. However, PdO dispersion (based on CO pulse chemisorption) was higher and PdO particle size was smaller in the 20CeO<sub>2</sub>-4Pd/Al<sub>2</sub>O<sub>3</sub> catalyst. This apparent anomaly in results could be explained by hypothesizing that the support alumina stabilized the PdO species and facilitated oxygen migration on the surface and from the bulk in the 4Pd-20CeO<sub>2</sub>/Al<sub>2</sub>O<sub>3</sub> catalyst. The lower activities in the 20CeO<sub>2</sub>-4Pd/Al<sub>2</sub>O<sub>3</sub> catalyst could be due to inaccessibility of PdO active sites for the surface reaction with methane and oxygen at low temperature due to strong PdO-ceria interactions.

This research opened up a possibility of altering the surface properties of catalysts by an innovative synthesis method. This could help in the development of better catalysts for combustion of hydrocarbons and carbon monoxide at lower temperatures. We could infer from our results that sequence of impregnation in the synthesis of catalysts could significantly change catalytic properties due to metal oxide–support interactions and such interactions could impact catalytic activities.

**Supplementary Materials:** The following are available online at <http://www.mdpi.com/2073-4344/10/9/976/s1>, Figure S1: Catalyst synthesis apparatus, Figure S2: Catalytic reactor unit, Figure S3: XPS in Ce3d regions for the two catalysts, Figure S4: XPS of two catalysts pre and post reaction in the Pd3d and Ce3d regions, Figure S5: STEM image and EDS mapping of 4Pd-20CeO<sub>2</sub>/Al<sub>2</sub>O<sub>3</sub> catalyst (Post reaction), Figure S6: HAADF-STEM and SEM images of 4Pd-20CeO<sub>2</sub>/Al<sub>2</sub>O<sub>3</sub> catalyst (Post reaction), Figure S7: PdO shapes and interfaces in 4Pd-20CeO<sub>2</sub>/Al<sub>2</sub>O<sub>3</sub> catalyst, Figure S8: PdO shapes and interfaces in 4Pd-20CeO<sub>2</sub>/Al<sub>2</sub>O<sub>3</sub> catalyst (Post reaction), Figure S9: HAADF-STEM and SEM images of 20CeO<sub>2</sub>-4Pd/Al<sub>2</sub>O<sub>3</sub> catalyst before reaction, Figure S10: PdO shapes and interface in 20CeO<sub>2</sub>-4Pd/Al<sub>2</sub>O<sub>3</sub> catalyst (Post reaction), Figure S11: Particle size of PdO in 4Pd-20CeO<sub>2</sub>/Al<sub>2</sub>O<sub>3</sub> catalyst, Figure S12: PdO particle sizes in 4Pd-20CeO<sub>2</sub>/Al<sub>2</sub>O<sub>3</sub> catalyst (Post reaction), Figure S13: PdO particle sizes in 20CeO<sub>2</sub>-4Pd/Al<sub>2</sub>O<sub>3</sub> catalyst, Figure S14: PdO particle sizes in 20CeO<sub>2</sub>-4Pd/Al<sub>2</sub>O<sub>3</sub> catalyst (Post reaction).

**Author Contributions:** D.R.F. prepared the catalysts, conducted activity and activation energy experiments, and calculated the particle sizes. M.P.B. did the characterization experiments (BET, CO pulse chemisorption, H<sub>2</sub>-TPR, and XPS) and made all Figures and Tables. D.R.F. and M.P.B. made equal contributions to this article. Y.D. did the STEM/SEM/EDS measurements and interpreted the data. M.Z.B. conducted the XRD experiments. A.C.B. conceptualized and managed the project as the PI. He also wrote the manuscript. D.R.F., M.P.B., and Y.D. edited the manuscript. All authors have read and agreed to the published version of the manuscript.

**Funding:** This research received no external funding.

**Acknowledgments:** Anil Banerjee received University Faculty research grants from Columbus State University and Domenica Fertil received small grants for student research.

**Conflicts of Interest:** The authors declare no conflict of interest.

## References

1. Monai, M.; Montini, T.; Gorte, R.J.; Fornasiero, P. Catalytic Oxidation of Methane: Pd and Beyond. *Eur. J. Inorg. Chem.* **2018**, *2018*, 2884–2893. [[CrossRef](#)]
2. Chen, J.; Arandiyán, H.; Gao, X.; Li, J. Recent Advances in Catalysts for Methane Combustion. *Catal. Surv. Asia* **2015**, *19*, 140–171. [[CrossRef](#)]
3. Simplício, L.M.T.; Brandão, S.T.; Sales, E.A.; Lietti, L.; Bozon-Verduraz, F. Methane combustion over PdO-alumina catalysts: The effect of palladium precursors. *Appl. Catal. B Environ.* **2006**, *63*, 9–14. [[CrossRef](#)]
4. Goodman, E.D.; Dai, S.; Yang, A.C.; Wrasman, C.J.; Gallo, A.; Bare, S.R.; Hoffman, A.S.; Jaramillo, T.F.; Graham, G.W.; Pan, X.; et al. Uniform Pt/Pd Bimetallic Nanocrystals Demonstrate Platinum Effect on Palladium Methane Combustion Activity and Stability. *ACS Catal.* **2017**, *7*, 4372–4380. [[CrossRef](#)]
5. Banerjee, A.C.; McGuire, J.M.; Lawnick, O.; Bozack, M.J. Low-temperature activity and PdO-PdOx transition in methane combustion by a PdO-PdOx/ $\gamma$ -Al<sub>2</sub>O<sub>3</sub> catalyst. *Catalysts* **2018**, *8*, 266. [[CrossRef](#)]
6. Colussi, S.; Trovarelli, A.; Cristiani, C.; Lietti, L.; Groppi, G. The influence of ceria and other rare earth promoters on palladium-based methane combustion catalysts. *Catal. Today* **2012**, *180*, 124–130. [[CrossRef](#)]
7. Ma, J.; Lou, Y.; Cai, Y.; Zhao, Z.; Wang, L.; Zhan, W.; Guo, Y.; Guo, Y. The relationship between the chemical state of Pd species and the catalytic activity for methane combustion on Pd/CeO<sub>2</sub>. *Catal. Sci. Technol.* **2018**, *8*, 2567–2577. [[CrossRef](#)]
8. Cargnello, M.; Jaén, J.J.D.; Garrido, J.C.H.; Bakhmutsky, K.; Montini, T.; Gámez, J.J.C.; Gorte, R.J.; Fornasiero, P. Exceptional Activity for Methane Combustion over Modular Pd@CeO<sub>2</sub> Subunits on Functionalized Al<sub>2</sub>O<sub>3</sub>. *Science* **2012**, *337*, 713–718. [[CrossRef](#)]
9. Li, L.; Zhang, N.; Wu, R.; Song, L.; Zhang, G.; He, H. Comparative Study of Moisture-Treated Pd@CeO<sub>2</sub>/Al<sub>2</sub>O<sub>3</sub> and Pd/CeO<sub>2</sub>/Al<sub>2</sub>O<sub>3</sub> Catalysts for Automobile Exhaust Emission Reactions: Effect of Core-Shell Interface. *ACS Appl. Mater. Interfaces* **2020**, *12*, 10350–10358. [[CrossRef](#)]
10. Rodrigues, L.M.T.S.; Silva, R.B.; Rocha, M.G.C.; Bargiela, P.; Noronha, F.B.; Brandão, S.T. Partial oxidation of methane on Ni and Pd catalysts: Influence of active phase and CeO<sub>2</sub> modification. *Catal. Today* **2012**, *197*, 137–143. [[CrossRef](#)]
11. Ramírez-López, R.; Elizalde-Martínez, I.; Balderas-Tapia, L. Complete catalytic oxidation of methane over Pd/CeO<sub>2</sub>-Al<sub>2</sub>O<sub>3</sub>: The influence of different ceria loading. *Catal. Today* **2010**, *150*, 358–362. [[CrossRef](#)]
12. Sun, M.; Hu, W.; Yuan, S.; Zhang, H.; Cheng, T.; Wang, J.; Chen, Y. Effect of the loading sequence of CeO<sub>2</sub> and Pd over Al<sub>2</sub>O<sub>3</sub> on the catalytic performance of Pd-only close-coupled catalysts. *Mol. Catal.* **2020**, *482*, 100332. [[CrossRef](#)]
13. Liu, X.; Liu, J.; Geng, F.; Li, Z.; Li, P.; Gong, W. Synthesis and properties of PdO/CeO<sub>2</sub>-Al<sub>2</sub>O<sub>3</sub> catalysts for methane combustion. *Front. Chem. Sci. Eng.* **2012**, *6*, 34–37. [[CrossRef](#)]
14. Yang, X.; Du, C.; Guo, Y.; Guo, Y.; Wang, L.; Wang, Y.; Zhan, W. Al<sub>2</sub>O<sub>3</sub> supported hybrid Pd-CeO<sub>2</sub> colloidal spheres and its enhanced catalytic performances for methane combustion. *J. Rare Earths* **2019**, *37*, 714–719. [[CrossRef](#)]
15. Colussi, S.; Trovarelli, A.; Vesselli, E.; Baraldi, A.; Comelli, G.; Groppi, G.; Llorca, J. Structure and morphology of Pd/Al<sub>2</sub>O<sub>3</sub> and Pd/CeO<sub>2</sub>/Al<sub>2</sub>O<sub>3</sub> combustion catalysts in Pd-PdO transformation hysteresis. *Appl. Catal. A Gen.* **2010**, *390*, 1–10. [[CrossRef](#)]
16. Onn, T.M.; Zhang, S.; Arroyo-Ramirez, L.; Xia, Y.; Wang, C.; Pan, X.; Graham, G.W.; Gorte, R.J. High-surface-area ceria prepared by ALD on Al<sub>2</sub>O<sub>3</sub> support. *Appl. Catal. B Environ.* **2017**, *201*, 430–437. [[CrossRef](#)]
17. Liu, L.; Corma, A. Metal Catalysts for Heterogeneous Catalysis: From Single Atoms to Nanoclusters and Nanoparticles. *Chem. Rev.* **2018**, *118*, 4981–5079. [[CrossRef](#)]
18. Ahmadi, M.; Mistry, H.; Cuenya, B.R. Tailoring the Catalytic Properties of Metal Nanoparticles via Support Interactions. *J. Phys. Chem. Lett.* **2016**, *7*, 3519–3533. [[CrossRef](#)]

19. Banerjee, A.C.; Golub, K.W.; Hakim, M.A.; Billor, M.Z. Comparative study of the characteristics and activities of Pd/ $\gamma$ -Al<sub>2</sub>O<sub>3</sub> catalysts prepared by vortex and incipient wetness methods. *Catalysts* **2019**, *9*, 336. [[CrossRef](#)]
20. Huang, F.; Chen, J.; Hu, W.; Li, G.; Wu, Y.; Yuan, S.; Zhong, L.; Chen, Y. Pd or PdO: Catalytic active site of methane oxidation operated close to stoichiometric air-to-fuel for natural gas vehicles. *Appl. Catal. B Environ.* **2017**, *219*, 73–81. [[CrossRef](#)]
21. Lan, L.; Chen, S.; Zhao, M.; Gong, M.; Chen, Y. The effect of synthesis method on the properties and catalytic performance of Pd/Ce<sub>0.5</sub>Zr<sub>0.5</sub>O<sub>2</sub>-Al<sub>2</sub>O<sub>3</sub> three-way catalyst. *J. Mol. Catal. A Chem.* **2014**, *394*, 10–21. [[CrossRef](#)]
22. Murata, K.; Kosuge, D.; Ohyama, J.; Mahara, Y.; Yamamoto, Y.; Arai, S.; Satsuma, A. Exploiting Metal-Support Interactions to Tune the Redox Properties of Supported Pd Catalysts for Methane Combustion. *ACS Catal.* **2020**, *10*, 1381–1387. [[CrossRef](#)]
23. Murata, K.; Ohyama, J.; Yamamoto, Y.; Arai, S.; Satsuma, A. Methane Combustion over Pd/Al<sub>2</sub>O<sub>3</sub> Catalysts in the Presence of Water: Effects of Pd Particle Size and Alumina Crystalline Phase. *ACS Catal.* **2020**, *10*, 8149–8156. [[CrossRef](#)]
24. Miller, J.B.; Malatpure, M. Pd catalysts for total oxidation of methane: Support effects. *Appl. Catal. A Gen.* **2015**, *495*, 54–62. [[CrossRef](#)]
25. Schwartz, W.R.; Pfefferle, L.D. Combustion of methane over palladium-based catalysts: Support interactions. *J. Phys. Chem. C* **2012**, *116*, 8571–8578. [[CrossRef](#)]
26. Feng, X.; Li, W.; Liu, D.; Zhang, Z.; Duan, Y.; Zhang, Y. Self-Assembled Pd@CeO<sub>2</sub>/ $\gamma$ -Al<sub>2</sub>O<sub>3</sub> Catalysts with Enhanced Activity for Catalytic Methane Combustion. *Small* **2017**, *13*, 1700941. [[CrossRef](#)]
27. Nilsson, J.; Carlsson, P.A.; Fouladvand, S.; Martin, N.M.; Gustafson, J.; Newton, M.A.; Lundgren, E.; Grönbeck, H.; Skoglundh, M. Chemistry of Supported Palladium Nanoparticles during Methane Oxidation. *ACS Catal.* **2015**, *5*, 2481–2489. [[CrossRef](#)]
28. Puigdollers, A.R.; Schlexer, P.; Tosoni, S.; Pacchioni, G. Increasing oxide reducibility: The role of metal/oxide interfaces in the formation of oxygen vacancies. *ACS Catal.* **2017**, *7*, 6493–6513. [[CrossRef](#)]
29. Sulmonetti, T.P.; Pang, S.H.; Claire, M.T.; Lee, S.; Cullen, D.A.; Agrawal, P.K.; Jones, C.W. Vapor phase hydrogenation of furfural over nickel mixed metal oxide catalysts derived from layered double hydroxides. *Appl. Catal. A Gen.* **2016**, *517*, 187–195. [[CrossRef](#)]
30. Ding, Y.; Chen, Y.; Pradel, K.C.; Zhang, W.; Liu, M.; Wang, Z.L. Domain structures and Pr co antisite point defects in double-perovskite. *Ultramicroscopy* **2018**, *193*, 64–70. [[CrossRef](#)]



© 2020 by the authors. Licensee MDPI, Basel, Switzerland. This article is an open access article distributed under the terms and conditions of the Creative Commons Attribution (CC BY) license (<http://creativecommons.org/licenses/by/4.0/>).